Single nucleus transcriptomics supports a role for CCNA2-induced human adult cardiomyocyte cytokinesis

Esmaa Bouhamida[1], Sangeetha Vadakke-Madathil[1#], Prabhu Mathiyalagan[4#], Amaresh K. Ranjan[1,2#], Cherrie D. Sherman[1], Paul E Miller[3], Andre Ghetti[3], Najah Abi-Gerges[3] and Hina W. Chaudhry[1*]

[1] Icahn School of Medicine at Mount Sinai, New York, NY 10029, USA
[2] Chicago College of Pharmacy, Midwestern University, Downers Grove, IL, USA 60515
[3] AnaBios Corporation, San Diego, CA 92109, USA
[4] Benthos Prime Central, TX, USA
[#] Contributed equally

* Correspondence to:

Hina W. Chaudhry, M.D., Cardiovascular Regenerative Medicine, Mount Sinai School of Medicine, One Gustave L. Levy Place, Box 1030, New York, NY 10029, Phone: 212-241-4104, Fax: 212-241-5510. hina.chaudhry@mssm.edu.

Abstract

Cyclin A2 (CCNA2) is a master regulatory gene of the cell cycle that is normally silenced in postnatal mammalian cardiomyocytes. We have previously demonstrated that it can induce significant cardiac repair in both small and large animals when delivered to the heart via a viral vector. To date, whether CCNA2 gene delivery can induce cytokinesis in isolated cardiomyocytes from adult human hearts has not been investigated. Therefore, we designed a human gene therapy vector featuring a replication-deficient, E1/E3-deleted human adenovirus five encoding human CCNA2 driven by the cardiac Troponin T promoter to enable the expression of CCNA2 in freshly isolated human cardiomyocytes. Utilizing time-lapse microscopy live imaging of cultured adult human cardiomyocytes isolated from a 21-year-old male, 41-year-old female, and 55-year-old male, we now report that human adult cardiomyocytes can be induced to undergo complete cytokinesis in response to CCNA2 gene delivery with preservation of sarcomere integrity in the resulting daughter cells. To elucidate the mechanistic underpinnings of CCNA2-dependent gene regulation in governing cardiomyocyte cytokinesis, we conducted single nucleus transcriptomics (snRNA-seq, 10X Genomics) analysis in hearts isolated from adult transgenic mice that constitutively express CCNA2 in cardiomyocytes (CCNA2-Tg) and non-transgenic mice (nTg). Remarkably, we identified a subpopulation of cardiomyocytes enriched with cytokinesis, proliferative, and reprogramming genes in hearts obtained from CCNA2-Tg mice as compared to hearts obtained from nTg mice. We also performed bulk RNA sequencing of human adult and fetal hearts, and we identified key reprogramming genes that are involved in CCNA2-induced cytokinesis. These results provide a compelling path forward for the clinical development of cardiac regenerative therapy based on strategic manipulation of the cardiomyocyte cell cycle.

Keywords: CCNA2; cytokinesis; single-nucleus RNA-Seq; cell cycle; heart regeneration

Introduction

The vast morbidity and mortality of heart disease is, in large part, attributed to the inability of adult human cardiomyocytes to divide in a clinically sufficient manner [1]. Scar formation via fibrosis is, therefore, the primary response to cardiac injury. Multitudes of molecular and cellular approaches have been investigated over the past 20 years aimed at regenerating the myocardium in various states of heart disease [2-5]. Studies centered on the use of stem cells have remained controversial given the marginal results noted in clinical trials of cardiovascular cell therapy, and

there has not been conclusive evidence of actual cardiomyocyte differentiation arising from the cell types used in these trials. Human embryonic stem (ES) cells and induced pluripotent (iPS) cells have been evaluated in non-human primate models of heart disease with the demonstrated ability of these cell types to differentiate, at the very least, to immature cardiomyocytes with the hope that they would undergo maturation *in vivo.* However, it remains to be seen whether these approaches may be translated for human therapy [5, 6]. Aside from the differentiation and generation of new cardiomyocytes, some technical concerns still need to be addressed, such as the propensity for arrhythmias noted in primate hearts treated with ES-derived and iPS-derived cardiomyocytes [6, 7].

There has been evidence of a low level of cardiomyocyte turnover in the healthy human heart, but it is very limited, and this ability declines with age [8, 9]. Thus, cardiac regeneration in response to injury such as myocardial infarction (MI) remains a challenging clinical problem with limited options at the doorstep of therapeutic translation. Evolution may not have favored adult mammals in this regard, but certain members of metazoan species are capable of heart regeneration, and these examples may perhaps serve to enlighten us. Urodele amphibians, such as the newt, retain a remarkable capacity to replace lost anatomical tissues through epimorphic regeneration [10]. This process relies on the local plasticity of differentiated cells near the region of injury and involves reentry to the cell cycle with loss of differentiated characteristics to generate a 'local progenitor cell' of restricted potentiality [10].

The adult zebrafish heart can regenerate up to 20% of its volume via a mechanism largely dependent on the proliferation of cardiomyocytes adjacent to the area of injury [11, 12]. However, zebrafish harboring a temperature-sensitive mutation in *mps1*, a gene encoding a mitotic checkpoint kinase [11], cannot regenerate the heart, and scarring and fibrosis are noted in the excised areas in a manner similar to the response of the human heart after injury [11-13]. These results imply that the loss of a single gene can avert cardiomyocyte mitosis and mitigate the normal regenerative process, thus permitting fibrosis to proceed unimpeded.

We have demonstrated that cyclin A2 is a 'master regulator' of the cardiomyocyte cell cycle [14]. Unlike other cyclins, cyclin A2 complexes with its cyclin-dependent kinase partners to mediate both of the two transitions of the cell cycle: G1-S and G2-M [15-17] and is silenced shortly after birth in mammalian cardiomyocytes [18-20]. We subsequently have shown that cyclin A2 mediates cardiac repair by inducing cardiomyocyte mitoses after MI in two small animal models of MI [21-23]. As molecular mechanisms may be widely divergent across species, we performed a therapeutic efficacy study of cyclin A2-mediated cardiac repair in a porcine model of MI as it closely mimics human anatomy and physiology [24]. Therapeutic delivery of CCNA2 one

week after MI in the porcine heart induced cardiomyocyte cell cycle activation *in vivo* with marked enhancement of cardiac function as noted with multimodality imaging, including magnetic resonance imaging. The experimental pigs also exhibited significantly decreased fibrosis, lack of cardiomyocyte hypertrophy, and a 55% increase in cardiomyocyte cell numbers in the peri-infarct zones. Using the same viral vector encoding CCNA2 that was delivered *in vivo*, cultured porcine adult cardiomyocytes were induced to undergo cytokinesis with preservation of sarcomere structure [24].

For the purposes of clinical translation, we designed the next-generation gene therapy vector using a cardiomyocyte-specific promoter, cardiac Troponin T (cTnT), driving human CCNA2 expression **(Suppl. Figure 1)**. We then sought to determine whether this cTnT-CCNA2 vector would induce human adult cardiomyocytes to undergo cytokinesis. We employed live imaging microscopy after dynamically labeling the sarcomere within the adult human cardiomyocytes. Additionally, we use single nucleus RNA-seq (snRNA-seq, 10x Genomics) to explore the molecular signaling mechanisms associated with CCNA2-induced cardiomyocyte cytokinesis.

Results

cTnT-CCNA2 adenovirus vector designed for therapeutic use induces expression of CCNA2 in cultured adult human cardiomyocytes.

The therapeutic use grade human CCNA2 adenovirus vector was designed to express human cyclin A2 (CCNA2) specifically in cardiomyocytes by cloning human cDNA (NCBI Reference Sequence: NM_001237.4; 374-1672 bp) downstream to the cardiac Troponin T (cTnT) promoter **(Supp. Figure 1A)**. The cultured adult human cardiomyocytes were transfected with cTnT-hCCNA2 (test) versus cTnT-eGFP (control) adenoviruses with MOI of 100 each for assessing the induced expression of CCNA2. We observed significantly increased expression of CCNA2 in the cultured adult human cardiomyocytes transfected with the test compared to the control adenovirus (**Supp. Figure 1B**). We utilized cTnT-H2B-GFP after cytokinesis had occurred to confirm the nuclei of the daughter cells belonged to cardiomyocytes.

Adenoviral vector-mediated expression of CCNA2 induces cytokinesis in cultured adult human cardiomyocytes.

To assess the effect of induced CCNA2 expression on cell division in adult human cardiomyocytes, we cultured adult human cardiomyocytes and studied cytokinesis *in vitro* by using live cell epifluorescence time-lapse microscopy. The adult human cardiomyocytes were

plated at equal densities and transfected with cTnT-hCCNA2, cTnT-eGFP and/or cTnT-H2B-GFP and CMV-α-act-mCherry adenoviruses (test) or with cTnT-eGFP and/or cTnT-H2B-GFP and CMV-α-act-mCherry adenoviruses (control). cTnT-eGFP and/or cTnT-H2B-GFP adenovirus was transfected in both groups to confirm the initial tracking of cardiomyocytes (green) during live cell epifluorescence microscopy. For delineation of sarcomeric structure in cardiomyocytes, cells from both groups were co-transfected with adenovirus containing α-act-mCherry, which was constructed to allow for proper folding of the virally delivered α-actinin into the live cardiomyocyte sarcomere (CMV-α-act-mCherry) and was successfully used in cultured adult porcine cardiomyocytes [24]. This strategy enables us to confirm cardiomyocyte identity by assessing the expression of eGFP before and after cytokinesis and tracking sarcomere dynamics during live cell imaging. This strategy is more accurate than antibody-based identification, which can result in artifacts and can only be used at a one-time point after cell fixation. We observed co-expression of eGFP (green) and α-actinin (red) in cultured adult cardiomyocytes **(Figure 2A** and **2E**; first panel). We performed time-lapse microscopic imaging of live cells to capture cardiomyocyte cytokinesis **(Figure 2A** and **2E**; still images from **movie S1)**. We calculated the cytokinetic index of adult human cardiomyocytes by counting cytokinetic events observed in 42 regions of interest (ROIs) **(Supp. Table1)**. The cytokinetic index was significantly higher in the test samples with cTnT-CCNA2 adenovirus transfection compared to control samples in the 41- and 55-year-olds **(Figure 2F)**. In contrast, no significant change in the cytokinetic events between test and control samples was observed in the 21-year-old patient's cardiomyocytes **(Figure 2F)**. Most remarkably, sarcomere structure was preserved in the daughter cells after cytokinesis **(Figure 2B**; upon magnification of a daughter cell, the presence of sarcomeric structure is easily noted). The daughter cells were further identified with the expression of eGFP and/or H2B-GFP (as they were originally also transfected with cTnT-eGFP and/or H2B-GFP) and noted to be mononuclear after they had been fixed and stained with DAPI **(Figure 2C** and **2E)**. Clusters of other cardiomyocytes with expression of eGFP that had not taken up the Ad5-α-act-mCherry could be seen adjacent to the daughter cells **(Figure 2C)**. To confirm cardiomyocyte differentiation and preservation of sarcomeric structure in both parent and daughter cells, we measured differentiation potential by subjecting the cardiomyocytes to calcium flux imaging with pacing of 0.5 Hz and 1 Hz current and detected α-act-mCherry and sarcomere structure by fluorescence microscopy, respectively **(Figure 3A)**. We observed that ~5% of Ad5-cTnT-hCCNA2 transfected adult human cardiomyocytes show active Ca++ mobilization **(Figure 3B)**. Subsequently, these cardiomyocytes were fixed with 4% paraformaldehyde, and fluorescence microscopy was carried out to detect α-act-mCherry. A representative magnified fluorescence micrograph of adult human cardiomyocyte

post-differentiation clearly shows a very distinct sarcomere structure **(Figure 3C)**. Furthermore, we carried out bulk RNA-sequencing in fetal and adult human hearts, and our transcriptomics analysis demonstrated increased expressions for calcium handling and contractility genes as well as sarcomere genes (*Ryr2, Atp2a2, Scn5a, Calmk2a, Calm1*, *Calm2, Neb, Ttn, and Tnnc1*) in adult human hearts compared to fetal human heart **(Figure 3D)**. Additionally, our bulk RNA-seq analysis of mouse hearts with constitutive CCNA2 expression in cardiomyocytes revealed downregulation of sarcomere assembly genes (*Neb, Ttn, and Tnnc1)* in CCNA2-Tg mice hearts. This suggests that CCNA2 triggers the sarcomere assembly genes during cell division, promoting proliferation **(Supp. Figure 2)**. Furthermore, CCNA2 appears to play a role in preserving sarcomere structure after cell division and mobilizing calcium post-cytokinesis, indicating a time-dependent function of CCNA2 in cardiomyocyte cell cycle regulation.

Single nucleus transcriptomic (snRNA-seq) analysis of CCNA2-Tg mouse hearts identifies CCNA2-induced reprogramming genes in a selective subset of cardiomyocytes.

To explore the full spectrum of CCNA2-induced cardiomyocyte cytokinesis in an unbiased manner, we performed snRNA-seq on hearts isolated from control non-transgenic (nTg) and CCNA2 constitutively expressing transgenic (CCNA2-Tg) adult mice. We included both male and female mice at 8-12 weeks old for our study. This extensive dataset allows the identification of critical differentially expressed genes in cellular clusters throughout the heart of both nTg and CCNA2-Tg mice, in which CCNA2 expression is high **(Figure 4A-B** and **Supp. Figure 3)**. Another significant advantage of snRNA-seq is its capability to capture reads from diverse cell types that are typically underrepresented or lost during enzymatic tissue digestion.

Data visualization using a tSNE plot of combined nuclei profiles from both nTg and CCNA2-Tg mice enabled us to identify and classify 16 major cell types' populations, including cardiomyocytes, endothelial cells, fibroblasts, cardiac, immune cells, neuronal cells **(Figure 4C,** and **4D)**. Additionally, we identified several common clusters between nTg and CCNA2-Tg mice **(Figure 4E, Supp. Figure 3)**. The distribution of these clusters differs between the nTg and CCNA2-Tg heart tissues **(Figure 4F, 4G, and 4I)**. For instance, endothelial-derived fibroblasts are increased while fibroblasts are decreased in CCAH2-Tg mice as compared to controls **(Figure 4F)**. Cell identities were confirmed through the expression of cell-specific marker genes [25]. Cardiomyocyte populations were identified by classical marker genes (*Actn2* and *Tnnc1*) in both nTg and CCNA2-Tg hearts. Cardiomyocytes that express an enhanced level of markers of contractility, including the *Ryr2*, are designated as mature cardiomyocytes [26].

Ventricular cardiomyocyte (vCMs) populations were identified by the enrichment of *Myl2* and *Myh7*. We identified 11 clusters of the vCM population common to both nTg and CCNA2-Tg hearts, however, each with different proportions of the nuclei profiles. Notably, the vCM1 and vCM5 were more prevalent in nTg hearts, whereas the vCM2, vCM3, vCM4, vCM6, vCM7, vCM8, vCM9, pro-vCM10, and the vCM11 were more abundant in CCNA2-Tg hearts **(Figure 4G).** For example, vCM1 comprised 42.18% of vCMs in nTg compared to 30.94% in the CCNA2-Tg hearts, and vCM5 made up 4.12% of vCMs in nTg versus 3.32% in CCNA2-Tg. Conversely, vCM2 accounted for 34.12% in nTg but 36.57% in CCNA-Tg hearts. Similarly, vCM3 was 2.99% in nTg versus 7.64% in CCNA2-Tg, vCM8 2.30% versus 3.77% in CCNA2-Tg, vCM9 1.64% in nTg versus 2.05% in CCNA2-Tg, pro-vCM10 was 1.60% in nTg versus 2.01% **(Figure 4I).**

The populations vCM1, vCM2, vCM4, vCM5, and vCM11 exhibit elevated expression of genes associated with more mature cardiomyocytes, particularly those involved in sarcomere development such as *Ttn*, and calcium handling and cardiac contractility genes like *Pln, Ryr2*, and *Pkp2, Kcnd2*, and *Tnni3k,* which regulates cardiomyogenesis and function [27]. Notably, vCM5 displays heightened levels of *Ebf2*, implicated in brown adipocyte differentiation [28], and *Lsamp*, which guides neuronal connections [29]. In contrast, vCM3 and vCM7 show increased expression of ATP synthase genes *Atp5b* and *Atp5g3. Efnb2* expression is prominent in vCMs4 and vCM8, indicating a shared gene expression signature with endothelial cells. Additionally, vCM8 expresses *Tnni3, Ahsa1*, and *Tagln2*. Exclusive expression of *Igfbp3* characterizes vCM9 as mid-phase cardiomyocytes.

Conversely, analyzing the transcriptomic profile of the Pro-vCM10 population reveals elevated expression of early-phase proliferative markers (thus the name “Pro”) and cell cycle genes, including *Mki67*, *Kif23, Top2a, Cdc20, Cdk2d, Cdk1, Prc1,* and *Bub1*. Additionally, it exhibits a heightened expression of *Stmn1*, which is implicated in mitotic cytokinesis pathways [30], and *Cd44,* a regulator of adhesion complex assembly [31]. This subcluster also displays immune markers such as *C1qa.* Remarkably, Pro-vCM10 is highly enriched in CCNA2-Tg mouse hearts compared to nTg mouse hearts **(Figure 4H)**. Subsequently, we scrutinized the transcriptomic profiles of the distinct cardiomyocyte subsets, with a particular focus on the proliferative vCM population, analyzing individual features, both in nTg and CCNA2-Tg hearts. We confirmed CCNA2 expression in cardiomyocytes, notably within the enriched proliferative subset identified in CCNA2-Tg hearts, along with the expression of cell cycle genes **(Figure 5A,** and **5B)**. This expression pattern remained consistent across the combined transcriptomic profiles of all subclusters **(Supp. Figure 4).** Additionally, CCNA2 increases cardiomyocytes number in the Tg mice **(Figure 5C)**, aligning with our previous findings in porcine models [24]. Consistently,

regarding the cell cycle genes, our bulk RNA-seq data from mouse nTg and CCNA2-Tg cardiomyocytes yielded comparable findings. Specifically, we observed elevated levels of *Ccnb1* in CCNA2-Tg cardiomyocytes compared to nTg cardiomyocytes, along with slight increases in Ccnb2, *Cdk1 and Cdk2* in CCNA2-Tg cardiomyocytes **(Figure 6).** Notably, *Cdk1* is the sole essential cyclin-dependent kinase (*CDK*), when complexed to Cyclin A2 promotes entry into mitosis, whereas Cyclin A2/Cdk2 is critical for the G1/S transition [14, 32, 33].

Therefore, the identification of this pro-vCM subcluster in CCNA2-Tg mice shows specific expressions of cardiomyocyte low levels of *Ryr2* **(Figure 7A)** and high expression proliferative markers (*Mki67* and *Kif23*) **(Figure 7B)**. In mature CCNA2-Tg mice, *Ryr2* expression is decreased compared to nTg mice where the cardiomyocytes express higher *Ryr2* **(Figure 7A)**. This implies greater cardiomyocyte maturation in nTg mice compared to CCNA2-Tg mice, where cardiomyocytes appear less mature and may be primed for dedifferentiation processes to facilitate proliferation and regeneration [34]. These findings align with our bulk RNA-seq results, wherein CCNA2-Tg cardiomyocytes show decreased *Ryr2* expression as well as enhanced expression of proliferation markers as compared to nTg cardiomyocytes **(Supp. Figure 5A,** and **5B**).

In our quest to comprehend CCNA2-induced cytokinesis events, we explored whether distinct cardiomyocyte subclusters exhibit gene expression associated with cytokinesis and/or reprogramming in CCNA2-Tg mice. Intriguingly, the pro-vCM population demonstrated elevated expression of key cytokinesis genes (such as *Aurkb, Anln, Sept7,* and *Rho,* among others), notably significantly higher expressions of *Rho* and *Aurka* in CCNA2-Tg compared to nTg mice **(Figure 7C)**. Furthermore, this pro-vCM subcluster exhibited heightened expression of reprogramming genes (including *Pou5f1, Klf4, Gata4, Myc,* and *Sox2*), with *Pou5f1* expression significantly increased in CCNA2-Tg hearts compared to nTg hearts. Interestingly, *Sox2* expression was absent in nTg mice, while Sox2 is expressed in CCNA2-Tg mice **(Figure 7C)**. Consistent with the observations derived from bulk RNA-seq analysis, the expression levels of genes associated with cytokinesis, and reprogramming were upregulated in CCNA2-Tg cardiomyocytes compared to nTg cardiomyocytes **(Supp. Figure5C,** and **5D)**. Moreover, adult CCNA2-Tg cardiomyocytes exhibit a greater number of upregulated genes compared to nTg cardiomyocytes in mice **(Supp. Figure 5E).** Pathway analysis reveals distinct enrichment in multiple pathways in CCNA2-Tg cardiomyocytes, including immune-related pathways, extracellular matrix organization, and signal transduction pathways, while others show significant downregulation. Notably, pathways associated with mitochondrial biogenesis, respiratory electron transport, ATP synthesis coupling, and apoptotic-factor-mediated response are markedly suppressed **(Supp. Figure 5F).** This underscores the challenge faced by immature fetal

mitochondria, which lack well-developed cristae for efficient electron transport chain (ETC) function, in effectively producing ATP [35].

On the other hand, it is noteworthy to mention that in the adult murine context, approximately 85–90% of cardiomyocytes exist in a binucleated state [36], indicating that the nuclear count does not precisely correspond to the cell count. Furthermore, the polyploidization of cardiomyocytes has been recognized as an impediment to heart regeneration [37]. It has been reported that binucleated cardiomyocytes re-entering the cell cycle fail to complete cytokinesis, thereby impeding the efficient regeneration of cardiac tissue following injury [38].

To investigate whether such reprogramming genes are downregulated in adult human hearts, we carried out bulk RNA-sequencing in fetal and adult human hearts. Transcriptomic analysis of human hearts revealed that a number of cytokinesis (*Aurkb*, *Anln*, *Sept7*, *Rho,* and others) and the reprogramming *(Klf4, Gata4, Myc, Sox2,* and others*)* genes induced in CCNA2-Tg mouse hearts were mostly decreased for expression in human adult hearts as compared to fetal human hearts **(Figure 7D)**. Differentially expressed genes in the adult heart were downregulated as compared to the fetal human heart (**Figure 7E)**. Moreover, pathway analysis demonstrated several different pathways upregulated in the adult human heart, including metabolism, calcium mobilization, and ion homeostasis, and downregulated pathways, including mitotic telophase/cytokinesis, regulation of the mitotic cell cycle, and myogenesis **(Figure 7F, and 7I).**

Our study establishes that CCNA2 induces expression of reprogramming genes, which ultimately enhances cardiomyocyte cytokinesis. These results provide a compelling pathway forward for the clinical development of cardiac regenerative therapy based on the manipulation of the cardiomyocyte cell cycle.

Discussion

Epimorphic regeneration is a conserved mechanism across evolutionary biology, permitting organ-specific tissue regeneration in a variety of metazoan phylogeny, including early postnatal mammals [38]. In fact, in human neonates, the ventricular myocardium responds to the pressure overload of congenital aortic stenosis through hyperplastic growth, yet the degenerative, calcific aortic stenosis of older patients elicits hypertrophic growth of the myocardium [39-42]. These clinical observations imply that the cell cycle repertoire of human neonatal cardiomyocytes is also intact, as cardiac growth is able to occur in a similar fashion to the embryonic heart. Moreover, the adult human heart is also capable of a very low rate of turnover [8], with diminishing rates of

turnover past childhood and adolescence, with cardiomyocyte cytokinesis not evident past age 20 [9].

Strategies to induce cardiomyocyte cytokinesis in adult human hearts are of critical need in order to face the growing public health crisis of congestive heart failure. To our knowledge, most cell therapy clinical trials in heart disease have provided inconsistent evidence of improvements in left ventricular ejection fraction, with a lack of evidence that cell types utilized actually differentiate into functional cardiomyocytes. To this end, we previously explored the effects of cell cycle manipulation in small and large animal models and successfully induced cardiomyocyte proliferation *in vivo* with significant enhancement of cardiac function in animal models [21-24]. In any translational plan to use cell cycle regulators for clinical use, precautions must be in place to prevent the expression of cell cycle activators in extra cardiac tissues due to the potential for oncogenic transformation [43]. This safety concern prompted us to explore methods of tissue-specific activation of cyclin A2. One such method was to design a next-generation viral vector in which a cardiomyocyte-specific promoter, cardiac Troponin T, drives the expression of human cyclin A2 (cTnT-hCCNA2). Human cardiomyocytes isolated from 21-, 41- and 55-year-olds who had died of noncardiac causes were cultured utilizing adult mammalian cardiomyocyte culture methods developed by our laboratory [24] and transfected with cTnT-hCCNA2. Cardiomyocytes from the 41- and 55-year-olds in the experimental wells underwent complete cytokinesis at a significantly higher frequency than the cardiomyocytes in the control wells. Based on our previous studies of rodent cardiomyocytes, we attribute the low rate of cytokinetic events we observed in the control wells to the reactivation of endogenous CCNA2 with the prolonged culture of cardiomyocytes. This is a phenomenon we have previously observed and quantified in rodent cardiomyocytes (unpublished data), and likely not correlated with the low turnover seen in human hearts as measured by 14C dating [8] as cytokinesis markers were not noted at all in human hearts over the age 20 by Kühn and colleagues [9]. Similarly, Frisén and colleagues [44] used stereological and 14C quantification techniques to measure cardiomyocyte exchange. They found that most cardiomyocytes were never exchanged and that the substantial replacement of existing cardiomyocytes were generated in the first 10 years of life, while the second decade of life focused on DNA polyploidization. Cardiomyocyte plasticity plays a key role in cardiac remodeling and repair in infarcted hearts [45]. Our snRNA-Seq also confirms heightened cardiomyocyte plasticity of Ccna2 transgenic mice as we note changes in gene expression involved in cell cycle progression and reprogramming. Calcium signaling is a fundamental pathway in the regulation of cell division, cardiac contractility, and remodeling [46-48]. The increase in the cytokinetic index in the test samples from 41- and 55-year-olds shows the ability of CCNA2 to stimulate intracellular

Ca++ mobilization. Of note, the transfected cTnT-hCCNA2 (test samples) cultured cardiomyocytes isolated from a 21-year-old male did not show a significant increase in cytokinetic index invoked by CCNA2 when compared to the control samples, which is consistent with reports of previous investigators [9, 44] that cell turnover and cell division can naturally occur at younger ages in humans.

SnRNA-seq has been used to identify transcriptomic changes occurring at the single-cell level, shedding light on the precise mapping of transcriptomics alterations in a cell-type specific manner in response to cellular stimulation or gene delivery [49]. Employing snRNA-seq in intact tissues enables the capturing of cell-specific transcriptomics changes in a more precise manner while maintaining the integrity of tissue responses, compared to isolated *in vitro* transcriptomics analyses. Our strategy of using snRNA-seq is to identify cardiomyocyte-specific changes in an *in vivo* setting in a clinically relevant CCNA2-Tg model, which allowed us to map specific changes to a subpopulation of cardiomyocytes, which would not have been captured by analyzing the transcriptome of the bulk tissue of isolated cardiomyocytes using bulk RNA-seq strategies.

Furthermore, the genes induced in the CCNA2-Tg model appear to be representing a common mechanism underlying cytokinesis in both male and female mice, consistent with observations in human male and female hearts. Given that we identified a subset of cardiomyocytes being reprogrammed into a more proliferative state, our next goal is to investigate this cardiomyocyte subset population more definitively. Once we define the transcriptomic state and its proliferative potential in greater detail, we will focus on recapitulating such proliferative cardiomyocytes both *in vitro* and *in vivo* to investigate whether targeting these specific subpopulations holds greater therapeutic potential than targeting the entire cardiomyocyte population. The use of computational resources is currently a pressing necessity to enhance our comprehension of the molecular mechanism behind the processes and expediting the utilization of innovative technologies in researching and developing new therapeutic strategies for cardiac diseases.

Limitations:

The findings presented above are very promising, and there are a few limitations that warrant consideration. Firstly, the use of freshly isolated human adult primary cardiomyocytes offers an ideal cellular model, but presents several challenges. There is a high susceptibility to cell death in culture which can hinder such experiments and a fair amount of biological variability in getting the cells to adhere to the petri dishes. Adherence is necessary to perform these cytokinesis experiments. Greater consistency with very rapid isolation from human cadavers and further

refinements of the culture methods may overcome these challenges. The use of adenovirus vectors is safe and they are being utilized in other gene therapies that have been clinically tested. Immunogenicity is a concern, and therefore there are ongoing investigations in our laboratory to explore alternative delivery strategies.

Materials and Methods

Ethics Statement

This study was conducted in accordance with the Declaration of Helsinki. This study used cardiomyocytes from adult human heart tissues provided by Anabios, San Diego, CA. The specimens used in this research are fully de-identified and therefore are exempt from ethics approval.

Culture of Adult Human Cardiomyocytes and *in vitro* Cytokinesis Study

Cardiomyocytes from adult human (21-year-old male, 41-year-old female, and 55-year-old male) heart tissue were isolated after enzymatic digestion at Anabios, San Diego, CA, and were shipped to our laboratory within 24 hours of isolation. Adult human cardiomyocytes were subjected to culture similar to our previously published adult porcine cardiomyocyte culture technique [24] with slight modification. In brief, upon arrival, cells were washed with serum-free DMEM media twice, and 105 cells were seeded in 100mm untreated polystyrene plates. Non-adherent cells were collected every 24 hours and centrifuged at 20Xg for 2 min at room temperature. Cell pellet was washed with serum-free DMEM and seeded on new polystyrene plates in modified Cardiomyocyte Culture Media (mod CMC) [24] formulated by adding 13% FBS, 2.5% horse serum, 1X nonessential amino acid, 1mM sodium pyruvate, penicillin (100 U/ml), streptomycin (100 mg/ml), and fungizone (0.5 mg/ml) to Dulbecco's modified Eagle's medium (DMEM)/F12 (50:50). Cells were washed every day with serum-free DMEM, re-seeded in new polystyrene plates and cultured for 3 days. On day 4, they were seeded in glass-bottom 24-well tissue culture plates for 20 days, with the medium changed every 4th day. The wells with cardiomyocytes exhibiting adhesion and spreading were selected. Cells in these wells were trypsinized and counted, and 10^3 cells per well were seeded in new glass bottom tissue culture plates. After 2 days of culture, cells were divided into two groups (test and control) and were transfected with adenoviruses. The test group was transfected with cTnT-hCCNA2 along with cTnT-eGFP and/or cTnT-H2B-GFP and CMV-α-act-mCherry adenoviruses while the control group was transfected with only cTnT-eGFP and/or cTnT-H2B-GFP and CMV-α-act-mCherry adenoviruses. The multiplicity of infection (MOI) of adenoviruses were adjusted to 180 in each well of test (with cTnT-hCCNA2; MOI 100, CMV-α-

act-mCherry; MOI 40 and cTnT-eGFP or cTnT-H2B-GFP; MOI 40) and control (cTnT-eGFP; MOI 140 and CMV-α-act-mCherry; MOI 40) group. After 48 hours of incubation, transfection was confirmed by observing the desired fluorescence in live cell imaging with Zeiss AxioVision Observer Z1 inverted microscope (Carl Zeiss). We also tested the differentiation potential (active calcium flux and sarcomere structure) of cardiomyocytes after cytokinesis *in vitro* by culturing them in agarose-based semi-solid medium for 2 weeks. Cardiomyocytes were subjected to calcium flux imaging with pacing of 0.5 Hz and 1 Hz current. Cells were fixed in 4% paraformaldehyde, and fluorescence microscopy was carried out to detect the α-act-mCherry and sarcomere structure.

Time-lapse microscopy

To capture cell division events in cardiomyocytes *in vitro*, we carried out live cell epifluorescence time-lapse microscopy as described earlier [24]. In brief, Zeiss AxioVision Observer Z1 (Carl Zeiss, Thornwood, NY, USA) inverted epifluorescence microscope in a humidified chamber in the presence of 5% CO_2 at 37°C was used to carry out time-lapse microscopy. Multiple random points with cells expressing eGFP (green) and mCherry (red) were selected in the test and control groups. The positions were marked with the “position-list” tool in the AxioVision microscopy software (AxioVision Release 4.7, Carl Zeiss). After the first cycle of imaging, only the channel for Texas red was used (for detection of mCherry) to acquire images for 72 hours. The fluorescein isothiocyanate (green) channel of the microscope was kept closed during the time-lapse imaging to avoid cell death from exposure to ultraviolet rays in this channel. Images were taken at intervals of 30 min. The objective lens of 10X was used for all time-lapse imaging. Time-lapse movies were generated after the end of each experiment and exported as MOV files. The time-lapse movies were analyzed, and cells that underwent successful cytokinesis were enumerated in each group. The % cytokinesis events were calculated for each position, and the graph was plotted.

Cell fixation and nuclear staining

After time-lapse microscopy, cells in the glass-bottom plate were fixed with 4% paraformaldehyde at room temperature for 20 min and were stored at 4°C. For nuclear staining, cells were washed with 1XPBS and permeabilized by incubating them in 0.5% Triton X-100 solution for 20 min at room temperature. Cells were washed three times with 1XPBS and incubated in DAPI solution (2.5 ⌠g/ml) for 5 min. Cells were washed twice with 1X PBS, and

imaging was carried out using a Zeiss AxioVision Observer Z1 inverted epifluorescence microscope.

Real-time quantitative PCR

Quantitative PCRs were performed in cultured cardiomyocytes transfected with cTnT-hCCNA2 (test) or cTnT-eGFP (control) adenovirus with similar MOI (MOI 100). “SYBR Green quantitative PCR protocol” on the “StepOnePlus” real-time PCR system (Applied Biosystems, CA) was used. The PCR protocol consisted of one cycle at 95°C for 2 min, 39 cycles at 95°C for 15 sec + 60°C for 1 min, and then 4°C on hold. Gene expression was determined by using the formula 2^(39-⊗⊗CT) with consideration of CT value 39 for a single transcript and with normalization to the endogenous control GAPDH.

Animal

Cyclin A2 transgenic mice (Jackson Laboratory, Bar Harbor, Maine) [14] adult males and females of 8-12 weeks old were maintained in a B6CBA background. Non-transgenic (wild-type) littermates were used as our controls. All manipulations were performed according to Institutional Animal Care and Use Guidelines.

Collection of CCNA2-Tg mouse hearts

Sample preparation for Single Nucleus RNA-sequencing (snRNA-seq)

Frozen heart tissues from CCNA2-Tg- and nTg adult mice, male and female, were minced and transferred into a Dounce homogenizer containing cold lysis buffer (Benthos Prime Central, TX, USA). Samples were homogenized gently, and nuclei were isolated. Nuclei were ensured to be free of clumps and debris by trypan blue staining under a microscope. Nuclei were then counted, and concentration was adjusted. 10x library concentration, insert size, and quantification were checked using Qubit, Agilent bioanalyzer, and q-PCR, respectively. For data Processing and Quality Control of 10x Sequencing of snRNA-seq, the reads were processed with CellRanger software (v.3.1.0) (10x Genomics) with the default parameters for each sample separately. This involved various steps, including alignment to a reference, collapsing of unique molecular identifiers (UMIs), UMI counting, and initial quality control procedures. The outcome of this process was the generation of filtered gene expression matrices that exclusively contained cellular barcodes. Subsequently, the Seurat R package (v.3.1.1) was employed to further enhance data quality control. Cell Ranger employs the STAR aligner for splicing-aware mapping of reads to the genome. It utilizes a transcript annotation GTF file to categorize the reads into

exonic, intronic, and intergenic regions based on whether the reads align confidently with the genome. Only confidently mapped, non-PCR duplicates with valid barcodes and UMIs were used to generate a gene-barcode matrix. The filtered_feature_bc_matrix generated by Cell Ranger was used for Seurat processing. Cell marker identification was carried out using the cell-specific markers [25] and the dataset provided at iRhythmics FairdomHub instance under https://fairdomhub.org/studies/739.

Human Fetal and Adult Hearts and RNA sequencing

Human fetal heart RNA (n=3 pooled, Cat #636532, Takara) and human adult heart RNA (n=4 pooled, Cat #636583, Takara) were used for bulk RNA sequencing. Briefly, total RNA was used for rRNA depletion, followed by directional library preparation and sequencing. The sequence reads were mapped to the human genome (GRCh38.110) using STAR [50] (version 2.7.9a). Using the mapped reads, the R package edgeR [51] (version 3.30.3) was employed to calculate counts per million (CPM) values and false discovery rate (FDR)-adjusted p-values obtained through the Benjamini–Hochberg method (Benthos Prime Central, TX, USA).

Pathway analysis

Pathway analysis was conducted using the Reactome pathway analysis tool. For this analysis, we used a list of genes identified from differential expression analyses under both nTg and CCNA2-Tg conditions, selecting those with a log2FC > / < 1 and a P value < 0.05. Fold enrichment was calculated to indicate the gene expression observed in our uploaded list compared to the expected list. Categories with a fold enrichment greater than 1 were considered overrepresented, while those with a fold enrichment less than 1 were considered underrepresented in our experiment.

Data availability

The processed single-cell data and the bulk RNA sequencing, including raw expression matrices and raw sequence files that support this research study's findings, are available on the Gene Expression Omnibus GSE249433 and GSE256519, respectively.

Statistical analysis

Statistical analyses were carried out employing the R package (version 3.30.3) and using the GraphPad Prism (version 8.2.1, GraphPad). Student t-test or one/ two-way analysis of variance

(ANOVA test) were used for normal distributions. Data are presented as means ± SEM unless otherwise indicated. Significance was considered to be $P < 0.05$.

Acknowledgment:

We thank Dr. Bernhard Kühn for his contribution of the cTnT-H2B-GFP utilized in this study.

Funding:

This work is supported by the NIH R01 HL150345; the NYSTEM C029565 and NYSTEM C32608GG.

Conflict of interests:

The authors report no conflict of interest. H.W.C. is the founder and equity holder of VentriNova, Inc. and is listed as the inventor of multiple patents regarding cyclin A2-mediated cardiac repair and caudal-related homeobox 2 cells for cardiac repair.

References:

1. Laflamme, M.A. and C.E. Murry, *Heart regeneration.* Nature, 2011. **473**(7347): p. 326-35.
2. Miyamoto, K., et al., *Direct In Vivo Reprogramming with Sendai Virus Vectors Improves Cardiac Function after Myocardial Infarction.* Cell Stem Cell, 2018. **22**(1): p. 91-103 e5.
3. Cuculich, P.S., et al., *Noninvasive Cardiac Radiation for Ablation of Ventricular Tachycardia.* N Engl J Med, 2017. **377**(24): p. 2325-2336.
4. Yoshida, Y. and S. Yamanaka, *Induced Pluripotent Stem Cells 10 Years Later: For Cardiac Applications.* Circ Res, 2017. **120**(12): p. 1958-1968.
5. Doppler, S.A., et al., *Mammalian Heart Regeneration: The Race to the Finish Line.* Circ Res, 2017. **120**(4): p. 630-632.
6. Shiba, Y., et al., *Allogeneic transplantation of iPS cell-derived cardiomyocytes regenerates primate hearts.* Nature, 2016. **538**(7625): p. 388-391.
7. Chong, J.J., et al., *Human embryonic-stem-cell-derived cardiomyocytes regenerate non-human primate hearts.* Nature, 2014. **510**(7504): p. 273-7.
8. Bergmann, O., et al., *Evidence for cardiomyocyte renewal in humans.* Science, 2009. **324**(5923): p. 98-102.
9. Mollova, M., et al., *Cardiomyocyte proliferation contributes to heart growth in young humans.* Proc Natl Acad Sci U S A, 2013. **110**(4): p. 1446-51.
10. Brockes, J.P. and A. Kumar, *Plasticity and reprogramming of differentiated cells in amphibian regeneration.* Nat Rev Mol Cell Biol, 2002. **3**(8): p. 566-74.
11. Poss, K.D., L.G. Wilson, and M.T. Keating, *Heart regeneration in zebrafish.* Science, 2002. **298**(5601): p. 2188-90.
12. Jopling, C., et al., *Zebrafish heart regeneration occurs by cardiomyocyte dedifferentiation and proliferation.* Nature, 2010. **464**(7288): p. 606-9.
13. Furtado, M.B., et al., *View from the heart: cardiac fibroblasts in development, scarring and regeneration.* Development, 2016. **143**(3): p. 387-97.

14. Chaudhry, H.W., et al., *Cyclin A2 mediates cardiomyocyte mitosis in the postmitotic myocardium.* J Biol Chem, 2004. **279**(34): p. 35858-66.
15. Nurse, P., *A long twentieth century of the cell cycle and beyond.* Cell, 2000. **100**(1): p. 71-8.
16. Pagano, M., et al., *Cyclin A is required at two points in the human cell cycle.* EMBO J, 1992. **11**(3): p. 961-71.
17. Sherr, C.J. and J.M. Roberts, *Inhibitors of mammalian G1 cyclin-dependent kinases.* Genes Dev, 1995. **9**(10): p. 1149-63.
18. Wang, B.J. and H.W. Chaudhry, *Regulation of Cardiomyocyte Division During Cardiac Regeneration.* Curr Cardiol Rep, 2023. **25**(7): p. 615-620.
19. Vadakke-Madathil, S. and H.W. Chaudhry, *Cardiac Regeneration: Time to Revisit Nature.* Circ Res, 2018. **123**(1): p. 24-26.
20. Yoshizumi, M., et al., *Disappearance of cyclin A correlates with permanent withdrawal of cardiomyocytes from the cell cycle in human and rat hearts.* J Clin Invest, 1995. **95**(5): p. 2275-80.
21. Cheng, R.K., et al., *Cyclin A2 induces cardiac regeneration after myocardial infarction and prevents heart failure.* Circ Res, 2007. **100**(12): p. 1741-8.
22. Woo, Y.J., et al., *Therapeutic delivery of cyclin A2 induces myocardial regeneration and enhances cardiac function in ischemic heart failure.* Circulation, 2006. **114**(1 Suppl): p. I206-13.
23. Woo, Y.J., et al., *Myocardial regeneration therapy for ischemic cardiomyopathy with cyclin A2.* J Thorac Cardiovasc Surg, 2007. **133**(4): p. 927-33.
24. Shapiro, S.D., et al., *Cyclin A2 induces cardiac regeneration after myocardial infarction through cytokinesis of adult cardiomyocytes.* Sci Transl Med, 2014. **6**(224): p. 224ra27.
25. Litvinukova, M., et al., *Cells of the adult human heart.* Nature, 2020. **588**(7838): p. 466-472.
26. Galow, A.M., et al., *Integrative Cluster Analysis of Whole Hearts Reveals Proliferative Cardiomyocytes in Adult Mice.* Cells, 2020. **9**(5).
27. Lai, Z.F., et al., *Overexpression of TNNI3K, a cardiac-specific MAP kinase, promotes P19CL6-derived cardiac myogenesis and prevents myocardial infarction-induced injury.* Am J Physiol Heart Circ Physiol, 2008. **295**(2): p. H708-16.
28. Rajakumari, S., et al., *EBF2 determines and maintains brown adipocyte identity.* Cell Metab, 2013. **17**(4): p. 562-74.
29. Wang, L., et al., *Polymorphisms of the tumor suppressor gene LSAMP are associated with left main coronary artery disease.* Ann Hum Genet, 2008. **72**(Pt 4): p. 443-53.
30. Liu, J., et al., *Aberrantly high activation of a FoxM1-STMN1 axis contributes to progression and tumorigenesis in FoxM1-driven cancers.* Signal Transduct Target Ther, 2021. **6**(1): p. 42.
31. Zhao, L., et al., *CD44 regulates vascular gene expression in a proatherogenic environment.* Arterioscler Thromb Vasc Biol, 2007. **27**(4): p. 886-92.
32. Xing, Z., et al., *Expression and prognostic value of CDK1, CCNA2, and CCNB1 gene clusters in human breast cancer.* J Int Med Res, 2021. **49**(4): p. 300060520980647.
33. Santamaria, D., et al., *Cdk1 is sufficient to drive the mammalian cell cycle.* Nature, 2007. **448**(7155): p. 811-5.
34. Beisaw, A. and C.C. Wu, *Cardiomyocyte maturation and its reversal during cardiac regeneration.* Dev Dyn, 2024. **253**(1): p. 8-27.

35. Ding, Q., Y. Qi, and S.Y. Tsang, *Mitochondrial Biogenesis, Mitochondrial Dynamics, and Mitophagy in the Maturation of Cardiomyocytes.* Cells, 2021. **10**(9).
36. Soonpaa, M.H., et al., *Cardiomyocyte DNA synthesis and binucleation during murine development.* Am J Physiol, 1996. **271**(5 Pt 2): p. H2183-9.
37. Gonzalez-Rosa, J.M., et al., *Myocardial Polyploidization Creates a Barrier to Heart Regeneration in Zebrafish.* Dev Cell, 2018. **44**(4): p. 433-446 e7.
38. Bersell, K., et al., *Neuregulin1/ErbB4 signaling induces cardiomyocyte proliferation and repair of heart injury.* Cell, 2009. **138**(2): p. 257-70.
39. Bouhamida, E., et al., *The Complex Relationship between Hypoxia Signaling, Mitochondrial Dysfunction and Inflammation in Calcific Aortic Valve Disease: Insights from the Molecular Mechanisms to Therapeutic Approaches.* Int J Mol Sci, 2023. **24**(13).
40. Leeuwenburgh, B.P., et al., *Chronic right ventricular pressure overload results in a hyperplastic rather than a hypertrophic myocardial response.* J Anat, 2008. **212**(3): p. 286-94.
41. Assey, M.E., et al., *Unexpected persistence into adulthood of low wall stress in patients with congenital aortic stenosis: is there a fundamental difference in the hypertrophic response to a pressure overload present from birth?* Circulation, 1987. **75**(5): p. 973-9.
42. Torp, K.H., *Congenital aortic stenosis with hyperplasia of the endocardium in the left ventricle.* Acta Pathol Microbiol Scand, 1951. **29**(2): p. 109-19.
43. Wang, J., et al., *Hepatitis B virus integration in a cyclin A gene in a hepatocellular carcinoma.* Nature, 1990. **343**(6258): p. 555-7.
44. Bergmann, O., et al., *Dynamics of Cell Generation and Turnover in the Human Heart.* Cell, 2015. **161**(7): p. 1566-75.
45. Gong, R., et al., *Regulation of cardiomyocyte fate plasticity: a key strategy for cardiac regeneration.* Signal Transduct Target Ther, 2021. **6**(1): p. 31.
46. Patergnani, S., et al., *Various Aspects of Calcium Signaling in the Regulation of Apoptosis, Autophagy, Cell Proliferation, and Cancer.* Int J Mol Sci, 2020. **21**(21).
47. Rosendo-Pineda, M.J., C.M. Moreno, and L. Vaca, *Role of ion channels during cell division.* Cell Calcium, 2020. **91**: p. 102258.
48. Liu, C., et al., *Alteration of calcium signalling in cardiomyocyte induced by simulated microgravity and hypergravity.* Cell Prolif, 2020. **53**(3): p. e12783.
49. Bode, D., et al., *Exploiting Single-Cell Tools in Gene and Cell Therapy.* Front Immunol, 2021. **12**: p. 702636.
50. Dobin, A., et al., *STAR: ultrafast universal RNA-seq aligner.* Bioinformatics, 2013. **29**(1): p. 15-21.
51. Robinson, M.D., D.J. McCarthy, and G.K. Smyth, *edgeR: a Bioconductor package for differential expression analysis of digital gene expression data.* Bioinformatics, 2010. **26**(1): p. 139-40.

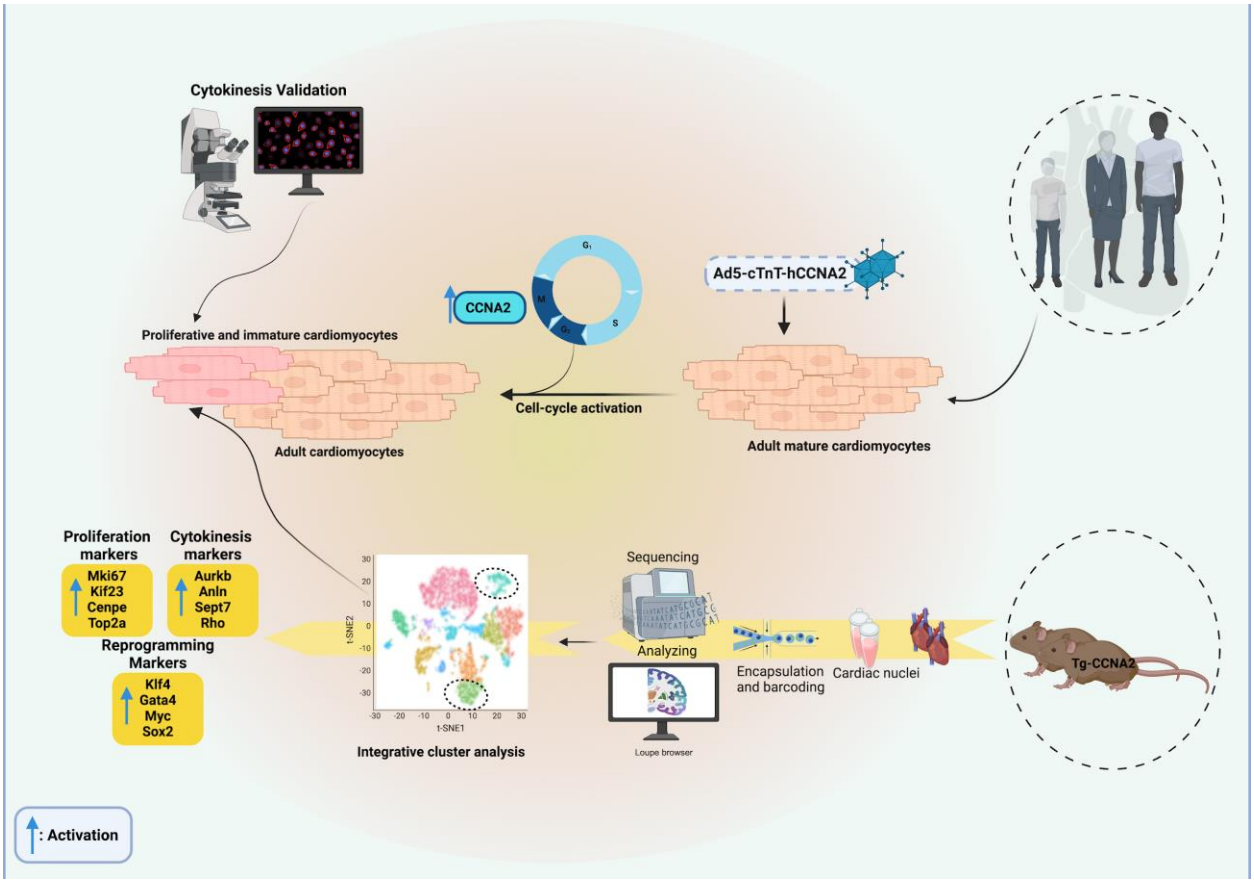

Figure 1: CCNA2 gene expression in primary adult cardiomyocytes induces cytokinesis while eliciting expression of proliferative and reprogramming genes in both humans and mice.

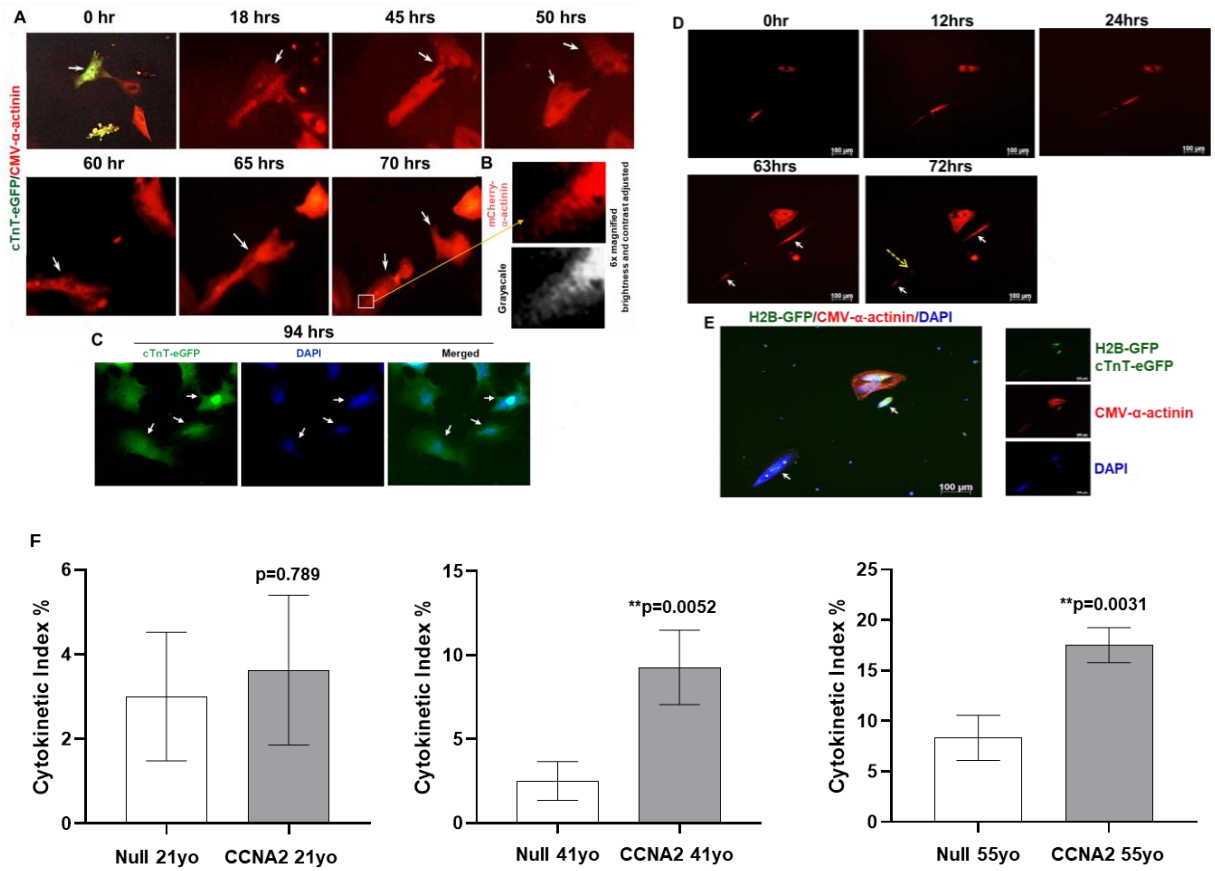

Figure 2: CCNA2 expression induces cytokinesis in adult human cardiomyocytes *In Vitro*. **A, D)** Still images from representative time-lapse epifluorescence microscopy of cultured cardiomyocytes isolated from adult humans (**A**. 55-, **E**. 41-year old). Cells were transfected with cTnT-hCCNA2, cTnT-H2B-GFP, cTnT-eGFP (to label cardiomyocytes), and CMV-α-actinin-m-Cherry adenoviruses prior to the beginning of the time-lapse imaging. At time 0 hr, a cell (yellow) expressing both Troponin Tc (green) and α-actinin (red) was followed for 70 hrs via time-lapse microscopy. The green channel was closed, and cells were only followed through the red channel to avoid UV photo-toxicity. The observed human cardiomyocytes show the 1st cell division at 50 hrs of imaging, and one of the daughter cells subsequently undergoes division at 70 hrs of imaging. **B)** At 70 hrs, a daughter cell is partially magnified with a grayscale version to demonstrate the presence of an intact sarcomere structure. **C, E)** One day after live imaging ended, these wells were fixed with subsequent labeling of nuclei with DAPI. The green fluorescence of the original cTnT-eGFP and cTnT-H2B-GFP transfection are visible, further confirming that these cells are cardiomyocytes. **F)** The cytokinetic events were counted in the control and test samples from the 21-, 41- and 55-year-old subjects. A significantly higher rate of cytokinesis was observed in the test samples from the 41 yo (2.5 ± 1.16 vs. 9.27 ± 2.22, p=0.005) and 51 yo (8.33 ± 2.25 vs. 17.52 ± 1.72, p=0.003) compared to the control. The control and test samples from the 21-year-old, on the other hand, did not exhibit a significant difference in the cytokinetic events (3.63 ± 1.77 vs 3.00 ± 1.52, p=0.789).

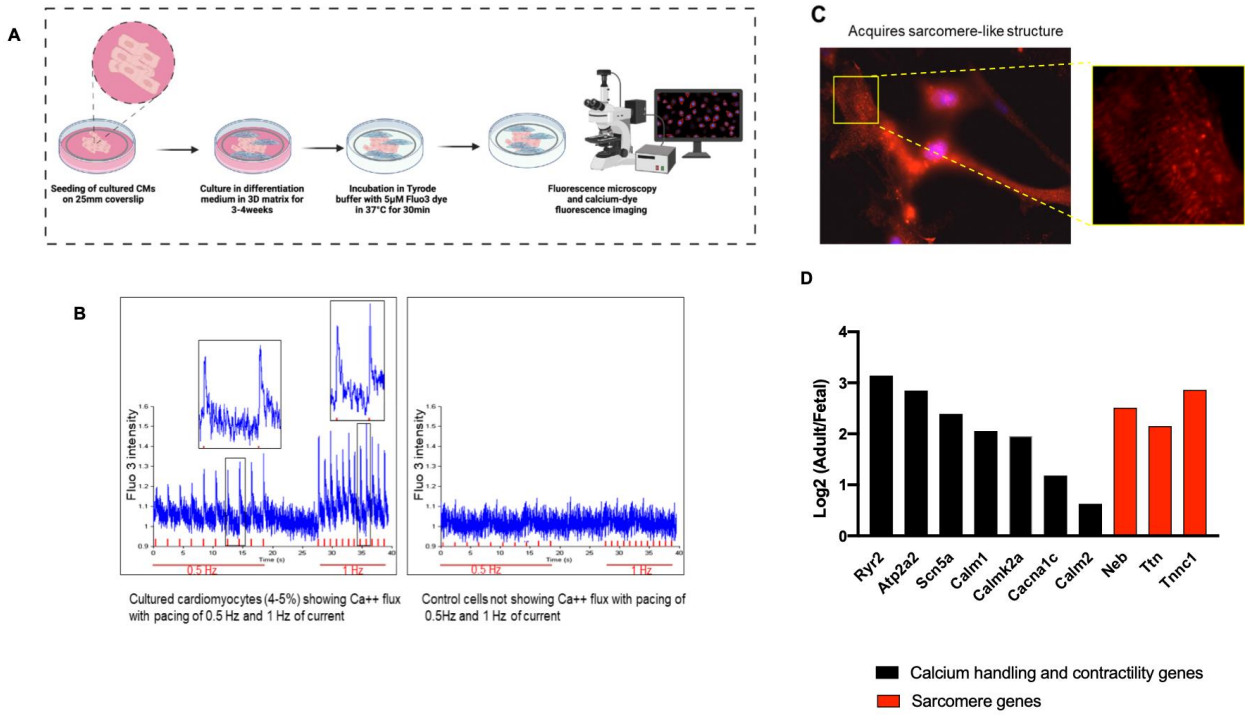

Figure 3: Differentiation of cultured adult human cardiomyocytes. Cultured adult human cardiomyocytes typically undergo dedifferentiation and were then subjected to 3D differentiation culture conditions and examined for calcium flux and re-appearance of the sarcomeric structure. **A)** Overview of the 3D culture method of differentiation, calcium flux measurement and fluorescence microscopy in adult human cardiomyocytes. **B)** Representative calcium flux graphs of re-differentiated cultured adult human cardiomyocytes. Approximately 4-5% of Ad5-cTnT-hCCNA2 transfected adult human cardiomyocytes show Ca++ flux with pacing of 0.5 and 1 Hz of current, while no calcium flux was detected in the non-Ad5-cTnT-hCCNA2 transfected cardiomyocytes. **C)** A representative cardiomyocyte image after re-differentiation. A randomly selected region of the imaged cardiomyocytes is magnified to demonstrate the presence of intact sarcomere structure after re-differentiation in 3D culture. **D)** Representative graph of calcium handling genes and contractility and sarcomere genes in adult and fetal human heart.

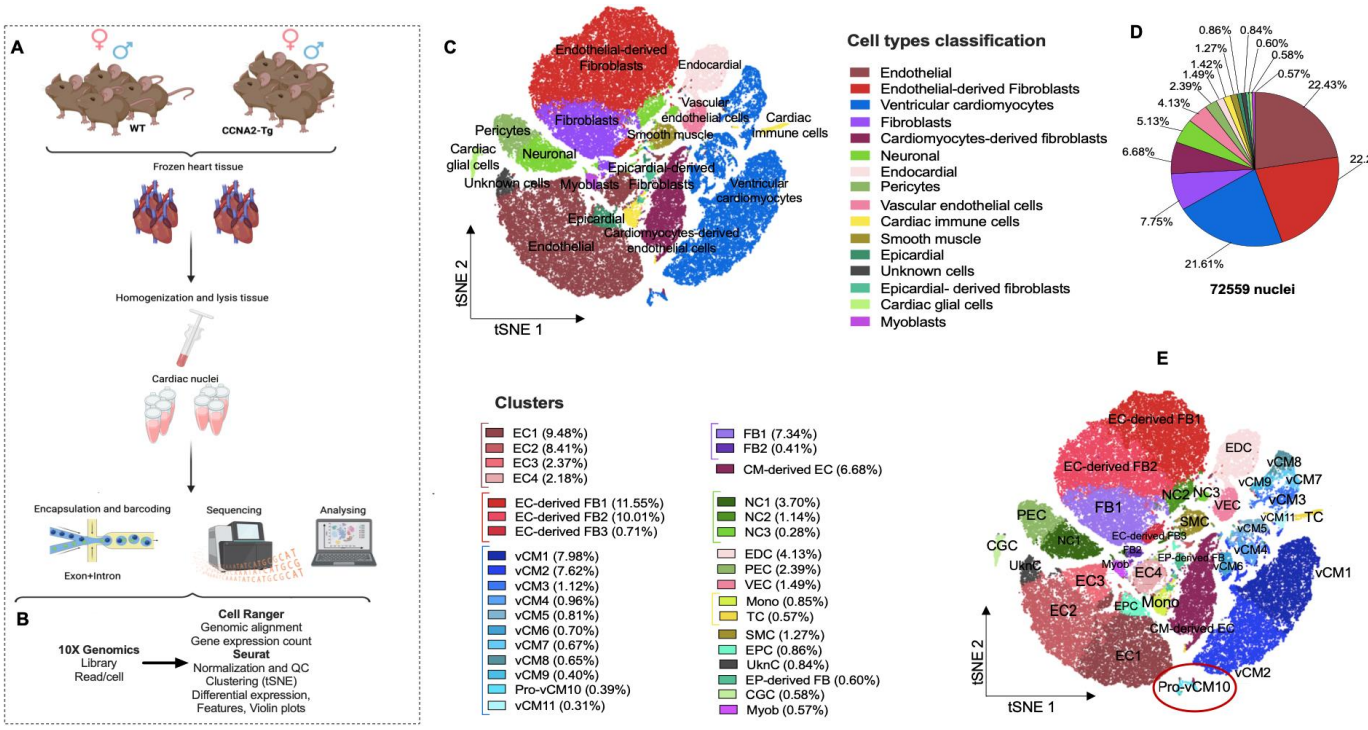

I

	nTg (%)	CCNA2-Tg (%)
vCM1	42.18	30.94
vCM2	34.12	36.57
vCM3	2.99	7.64
vCM4	4.28	4.62
vCM5	4.12	3.32
vCM6	3.02	3.53
vCM7	2.43	3.87
vCM8	2.30	3.77
vCM9	1.64	2.05
pro-vCM10	1.60	2.01
vCM11	1.28	1.63

Figure 4: **Single nucleus RNA sequencing identified major cell-types in CCNA2-Tg mice**
A) Schematic depicting the design of the snRNA-seq experiments (n=2) for each condition nTg female, CCNA2-Tg female, nTg male, and nTg male. **B)** The analysis pipeline and single-cell barcoded library generation (10X Genomics), sequence alignment (Cell Ranger), and further analysis using R (SeuratR package). **C)** t-distributed Stochastic Neighbor Embedding (tSNE) clustering the nuclei and reveals more 16 distinct major cell types identified based on the cell-specific markers dataset provided at iRhythmics FairdomHub instance and **D)** the pie chart showing the proportion of cells within the snRNA-seq. **E)** t-distributed Stochastic Neighbor Embedding (tSNE) of a total of 35 subclusters. **F)** Proportion of the nuclei in each cell type in percentage, and **I)** in each cluster and in all ventricular cardiomyocytes in both CCNA2-Tg and nTg mice. CM: Cardiomyocytes, vCM: ventricular cardiomyocytes, EC: endothelial cells, Ec-derived FB: endothelial derived fibroblasts; FB: fibroblasts, NC: neuronal, EDC: endocardial cells., PEC: pericytes, VEC: vascular endothelial cells, Mono: monocytes, TC: T-Cells, SMC: smooth muscle cells, EPC: epicardial cells, UnkC: unknown cells, EP-derived fb: epicardial derived fibroblasts, CGC: Cardiac glial cells, Myob: myoblasts.

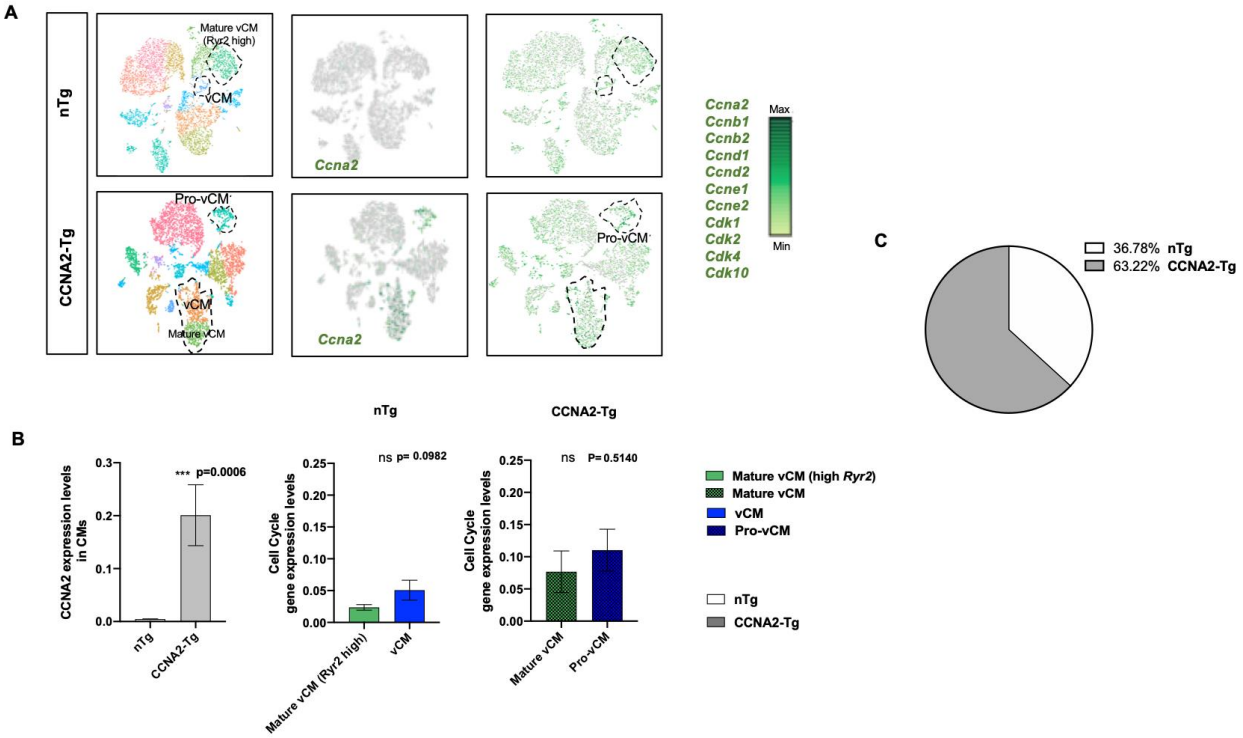

Figure 5: CCNA2 expression in cardiomyocytes of CCNA2-Tg and nTg mice delineated by snRNA-seq. A) CCNA2 expressed in a the pro-vCM subset of the cardiomyocyte population in CCNA2-Tg and cell cycle genes projected on the tSNE plot. **B)** Representative bar graph showing CCNA2 and cell cycle genes expression level in cardiomyocytes of CCNA2-Tg and nTg mice.

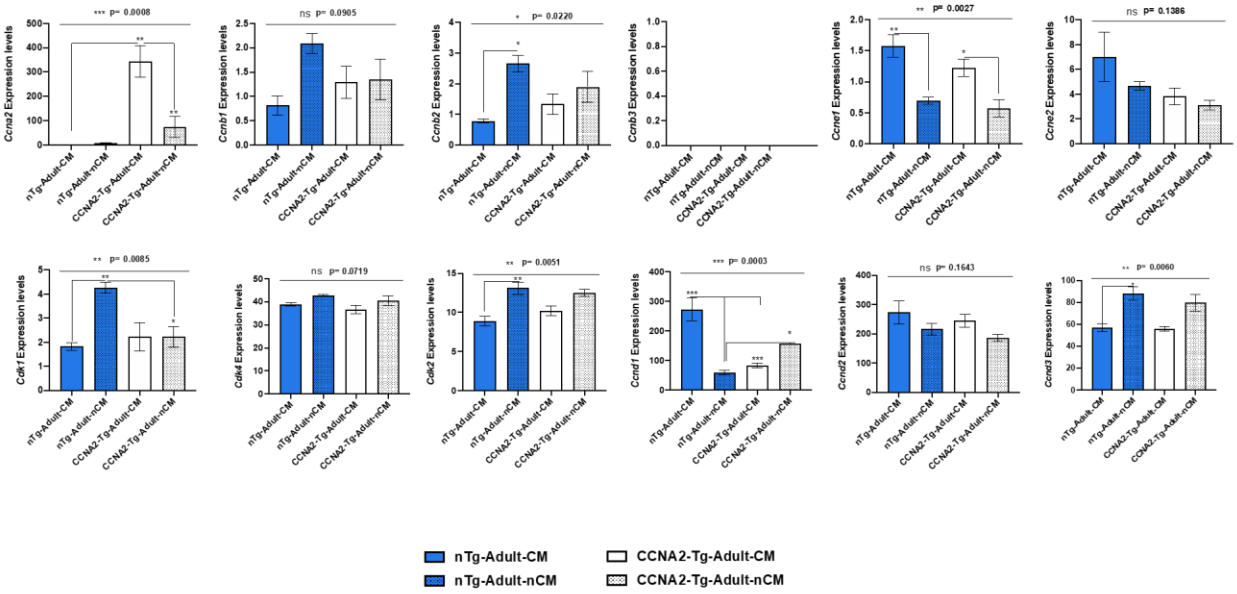

Figure 6: Cell cycle gene expression delineated by the bulk RNA-seq from mouse CCNA2-Tg and nTg cardiomyocytes. Bar graphs representing multiple cell cycle gene expression (*Ccna2, Cdk1, Cdk2, Cdk4, Ccnb1, Ccnb2, Ccnb3, Ccne1, Ccne2, Ccnd1, Ccnd2,* and *Ccnd3*) in nTg and CCNA2-Tg adult cardiomyocytes and non-cardiomyocytes.

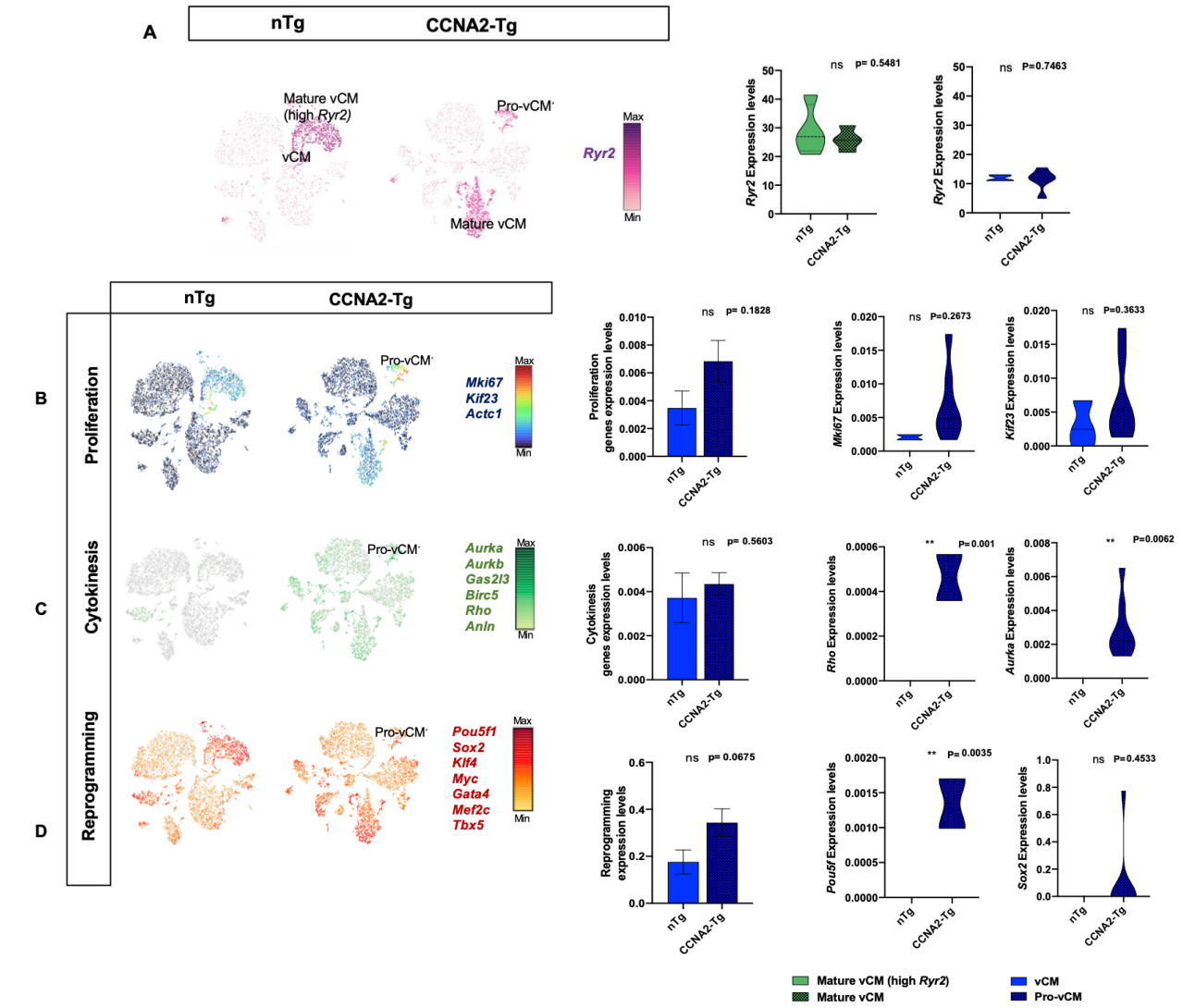
A
nTg
CCNA2-Tg
Mature vCM (high Ryr2)
vCM
Pro-vCM
Mature vCM
Ryr2
Max
Min
Ryr2 Expression levels
ns p= 0.5481
ns P=0.7463
B
Proliferation
Mki67
Kif23
Actc1
Proliferation genes expression levels
ns p= 0.1828
ns P=0.2673
ns P=0.3633
C
Cytokinesis
Aurka
Aurkb
Gas2l3
Birc5
Rho
Anln
Cytokinesis genes expression levels
ns p= 0.5603
** P=0.001
** P=0.0062
D
Reprogramming
Pou5f1
Sox2
Klf4
Myc
Gata4
Mef2c
Tbx5
Reprogramming expression levels
ns p= 0.0675
** P= 0.0035
ns P=0.4533
nTg
CCNA2-Tg
Mature vCM (high Ryr2)
Mature vCM
vCM
Pro-vCM

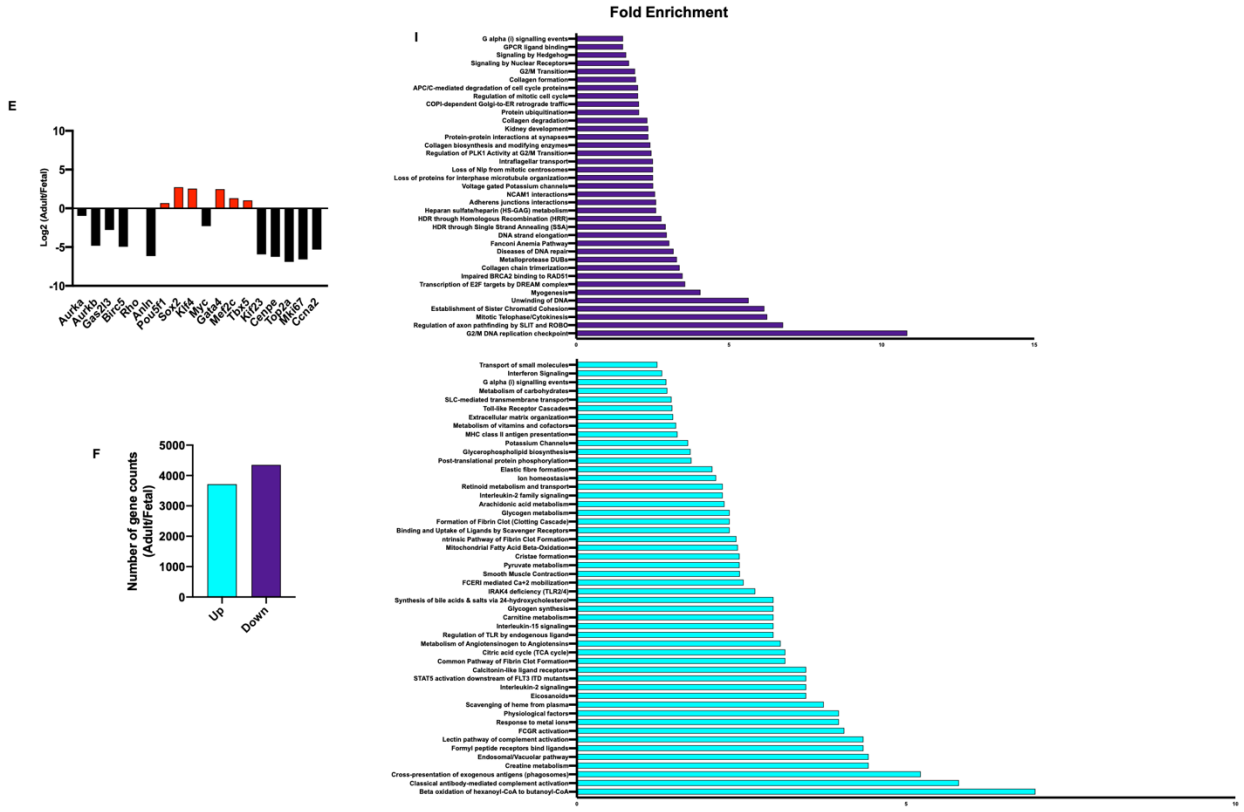
E
Log2 (Adult/Fetal)
Aurka
Aurkb
Gas2l3
Birc5
Rho
Anln
Pou5f1
Sox2
Klf4
Myc
Gata4
Mef2c
Tbx5
Kif23
Cenpe
Top2a
Mki67
Ccna2
F
Number of gene counts (Adult/Fetal)
Up
Down
I
Fold Enrichment
G alpha (i) signalling events
GPCR ligand binding
Signaling by Hedgehog
Signaling by Nuclear Receptors
G2/M Transition
Collagen formation
APC/C-mediated degradation of cell cycle proteins
Regulation of mitotic cell cycle
COPI-dependent Golgi-to-ER retrograde traffic
Protein ubiquitination
Collagen degradation
Kidney development
Protein-protein interactions at synapses
Collagen biosynthesis and modifying enzymes
Regulation of PLK1 Activity at G2/M Transition
Intraflagellar transport
Loss of Nlp from mitotic centrosomes
Loss of proteins for interphase microtubule organization
Voltage gated Potassium channels
NCAM1 interactions
Adherens junctions interactions
Heparan sulfate/heparin (HS-GAG) metabolism
HDR through Homologous Recombination (HRR)
HDR through Single Strand Annealing (SSA)
DNA strand elongation
Fanconi Anemia Pathway
Diseases of DNA repair
Metalloprotease DUBs
Collagen chain trimerization
Impaired BRCA2 binding to RAD51
Transcription of E2F targets by DREAM complex
Myogenesis
Unwinding of DNA
Establishment of Sister Chromatid Cohesion
Mitotic Telophase/Cytokinesis
Regulation of axon pathfinding by SLIT and ROBO
G2/M DNA replication checkpoint
Transport of small molecules
Interferon Signaling
G alpha (i) signalling events
Metabolism of carbohydrates
SLC-mediated transmembrane transport
Toll-like Receptor Cascades
Extracellular matrix organization
Metabolism of vitamins and cofactors
MHC class II antigen presentation
Potassium Channels
Glycerophospholipid biosynthesis
Post-translational protein phosphorylation
Elastic fibre formation
Ion homeostasis
Retinoid metabolism and transport
Interleukin-2 family signaling
Arachidonic acid metabolism
Glycogen metabolism
Formation of Fibrin Clot (Clotting Cascade)
Binding and Uptake of Ligands by Scavenger Receptors
ntrinsic Pathway of Fibrin Clot Formation
Mitochondrial Fatty Acid Beta-Oxidation
Cristae formation
Pyruvate metabolism
Smooth Muscle Contraction
FCERI mediated Ca+2 mobilization
IRAK4 deficiency (TLR2/4)
Synthesis of bile acids & salts via 24-hydroxycholesterol
Glycogen synthesis
Carnitine metabolism
Interleukin-15 signaling
Regulation of TLR by endogenous ligand
Metabolism of Angiotensinogen to Angiotensins
Citric acid cycle (TCA cycle)
Common Pathway of Fibrin Clot Formation
Calcitonin-like ligand receptors
STAT5 activation downstream of FLT3 ITD mutants
Interleukin-2 signaling
Eicosanoids
Scavenging of heme from plasma
Physiological factors
Response to metal ions
FCGR activation
Lectin pathway of complement activation
Formyl peptide receptors bind ligands
Endosomal/Vacuolar pathway
Creatine metabolism
Cross-presentation of exogenous antigens (phagosomes)
Classical antibody-mediated complement activation
Beta oxidation of hexanoyl-CoA to butanoyl-CoA

Figure 7: CCNA2 expression induces proliferation, cytokinesis, and reprogramming in mouse cardiomyocytes. A) *Ryr2* expression projected on tSNE and representative bar of its expression levels in cardiomyocytes types (more mature state expressing high *Ryr2*, less mature, ventricular cardiomyocytes and proliferative cardiomyocytes) in CCNA2-Tg. **B)** t-distributed Stochastic Neighbor Embedding (tSNE) and Representative graph and Violin plot representing the expression proliferation, **C)** cytokinesis and **B)** reprogramming markers in both CCNA2-Tg and nTg mice. **E)** Representative bar graph showing downregulated and upregulated gene of proliferation, cytokinesis and reprogramming genes level in human adult versus fetal hearts. **F)** Bar graph representing the up or down regulated genes in human adult versus fetal heart. **I)** enrichment analyses representing (on top) the downregulated pathways in Human Adult Heart, 4348 downregulated genes in human adult hearts were used to determine pathways downregulated, Top pathways shown, p<0.05; and Upregulated pathways in Human Adult Heart, representing 3713 upregulated genes in human adult hearts were used to determine pathways upregulated, Top 50 pathways shown, p<0.05.

Integrated supplementary information

Movie (attached): The real-time, live-imaging movie of human adult cardiomyocytes (55-year-old male) is described in **Figure 2**.

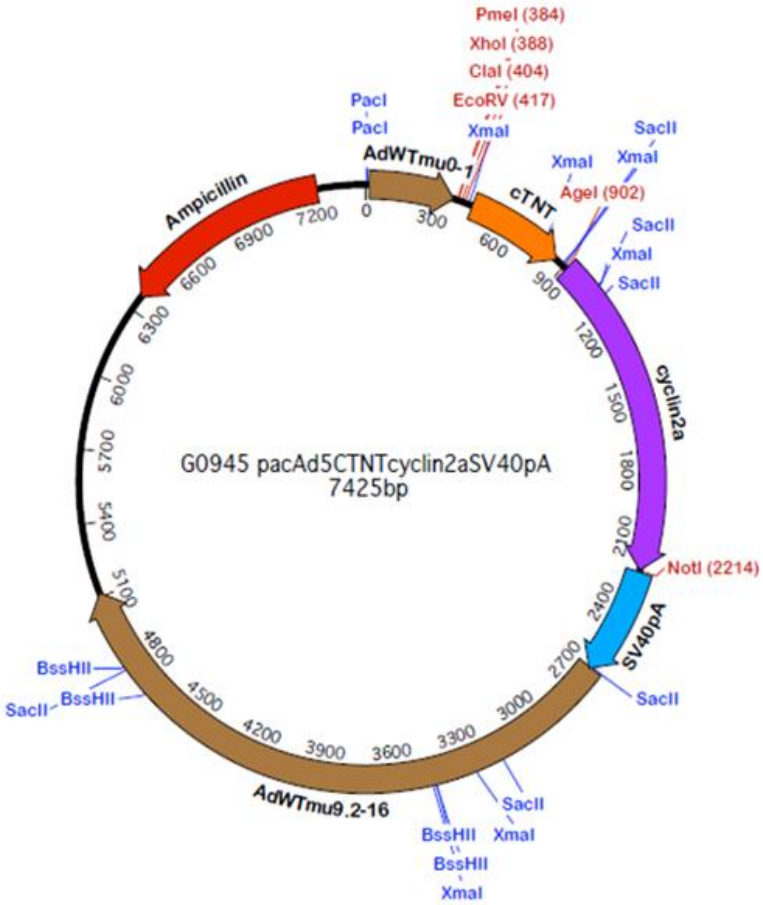

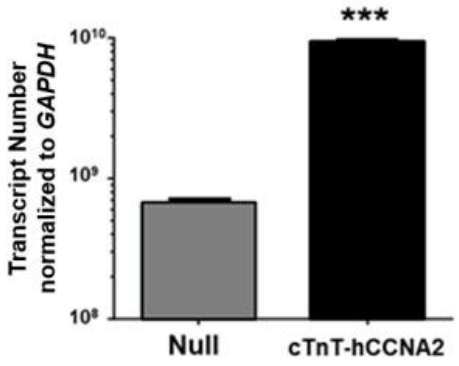

Supplementary Figure 1: Adenovirus vector construct and CCNA2 expression in adult human cardiomyocytes *in vitro*. **A)** Clinical-use grade replication-deficient human adenovirus type 5 (Ad5) was used for this study. The vector was designed with cardiac Troponin T (cTnT) promoter to express human cyclin A2 (hCCNA2) specifically in cardiomyocytes. **B)** The cTnT-hCCNA2 adenovirus was used to transfect cultured adult human cardiomyocytes to induce the expression of CCNA2. Significantly higher CCNA2 expression was observed in cells transfected with cTnT-hCCNA2 compared to the control virus.

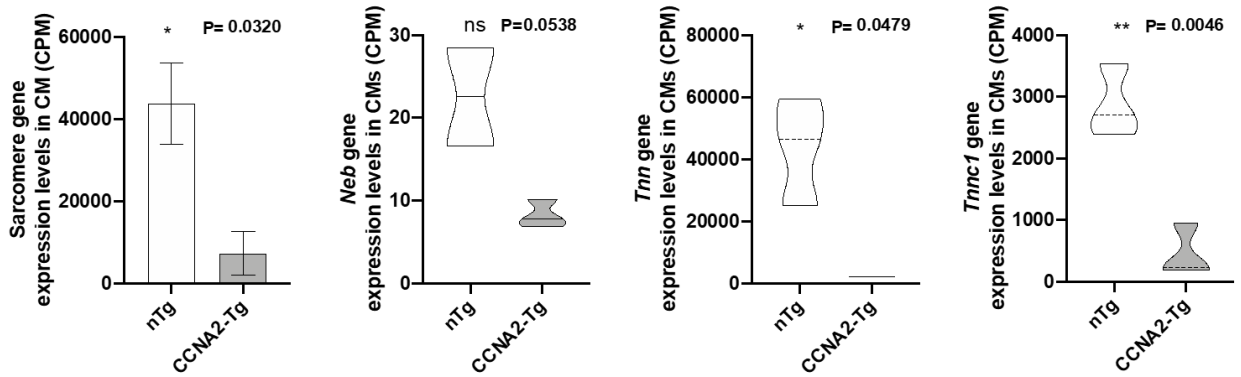

Supplementary Figure 2: Representative graphs of sarcomere assembly genes *(Neb, Tnn,* and *Tnnc1)* in nTg and CCNA2-Tg cardiomyocytes as delineated from bulk RNA seq.

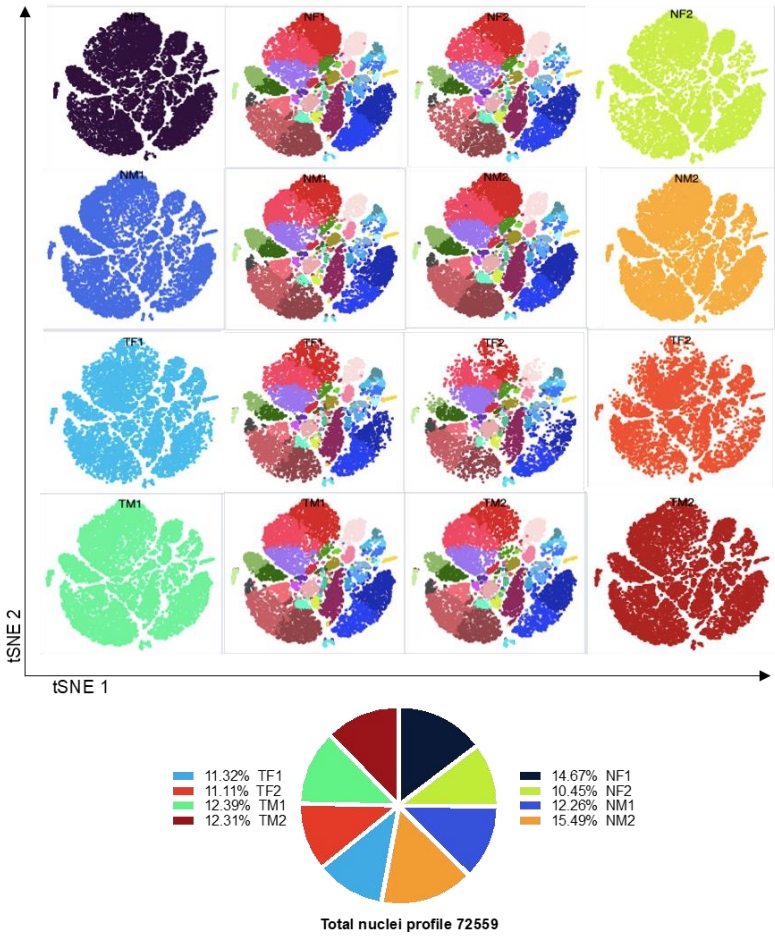

Supplementary Figure 3: t-distributed Stochastic Neighbor Embedding (tSNE) plot clustering the nuclei of nTg and CCNA2-Tg conditions (n=8 total). Chart Pie representing the percentage of nuclei profile in all conditions of nTg and CCNA2-Tg mice.

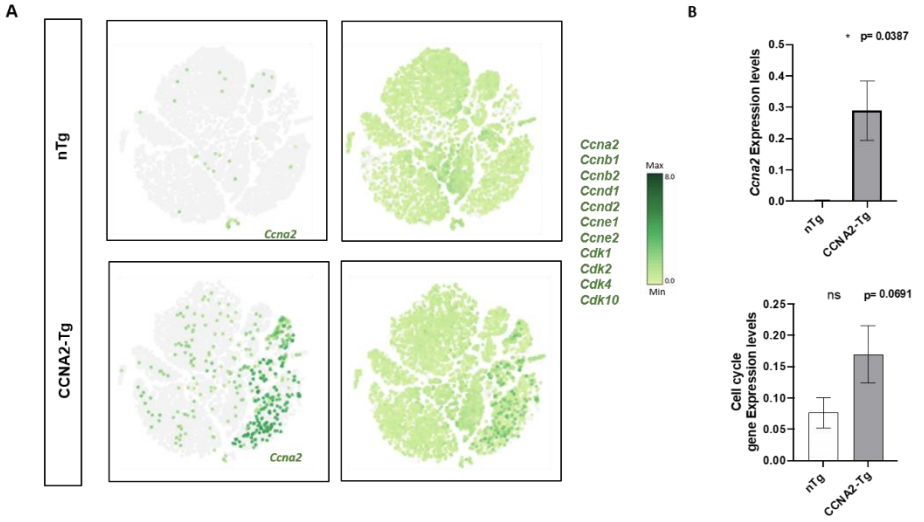

Supplementary Figure 4: CCNA2 and cell cycle genes expression across the combined transcriptomic profiles of all subclusters of nTg and CCNA2-Tg mice.

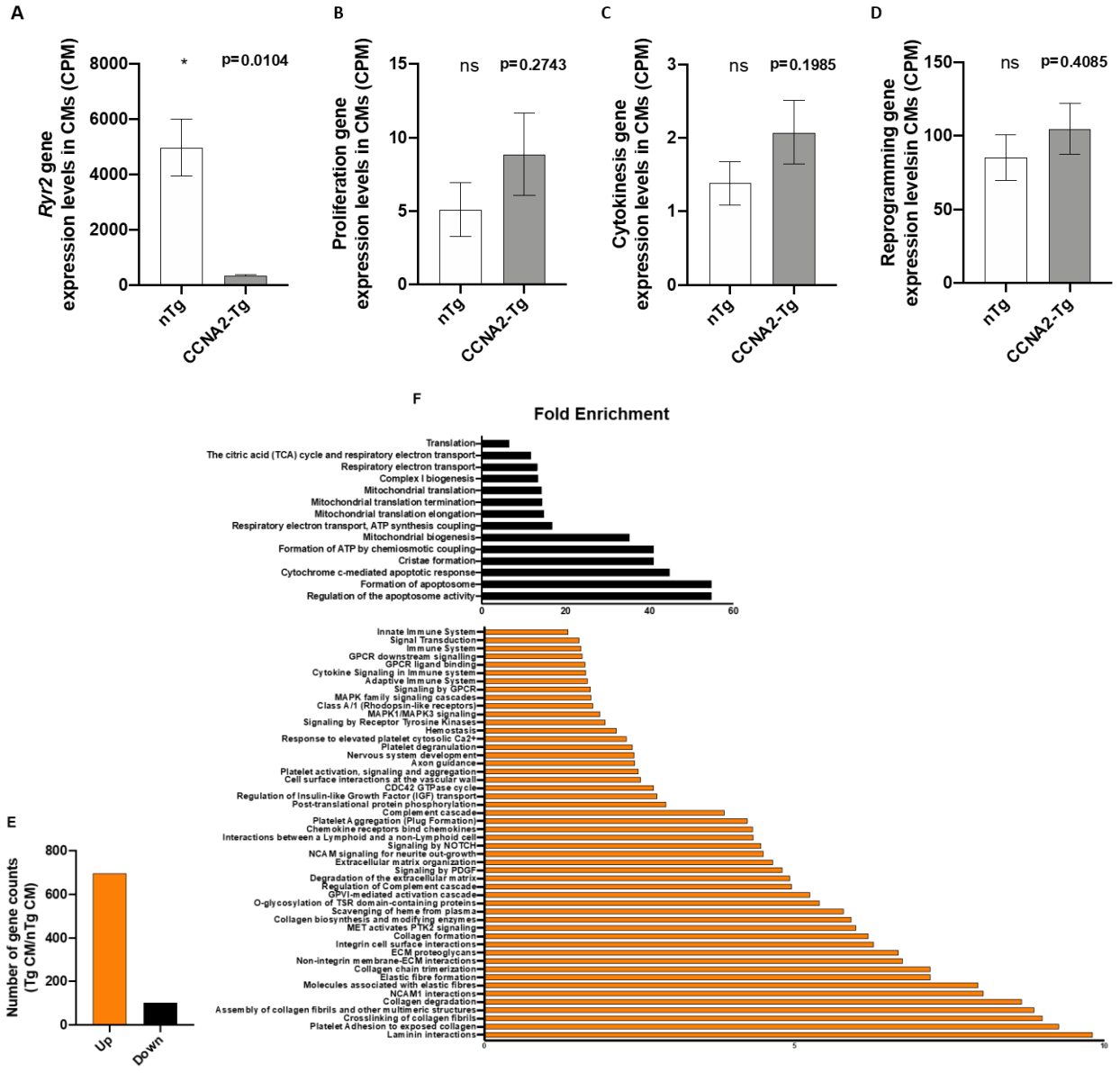

Supplementary Figure 5: Representative graphs of **A)** cardiomyocytes maturation gene *Ryr2, B)* proliferation, **C)** cytokinesis and **D)** reprogramming genes expression in nTg and CCNA2-Tg cardiomyocytes. **E)** Number of differentially expressed genes (Up or Down) in adult CCNA2-Tg mouse cardiomyocytes as compared to adult nTg mouse cardiomyocytes. **F)** Fold enrichment pathways in adult CCNA2-Tg mouse cardiomyocytes, with upregulated pathways shown in orange and downregulated genes in black.

Supplementary table 1 (Table S1): Table of raw data of cytokinesis events in regions of interest (ROIs) for experimental and control wells.

Test (cTNT-CCNA2+cTNT-eGFP)				Control (cTNT-eGFP only)			
ROI	Number of cells	Cytokinetic events	(%)	ROI	Number of cells	Cytokinetic events	(%)
ROI 1	23	5	21.7	ROI 29	13	1	7.7
ROI 2	7	1	14.3	ROI 30	33	1	3.0
ROI 3	17	4	23.5	ROI 31	21	1	4.8
ROI 4	24	7	29.2	ROI 32	9	3	33.3
ROI 5	12	5	41.7	ROI 33	27	3	11.1
ROI 6	11	2	18.2	ROI 34	33	1	3.0
ROI 7	20	4	20.0	ROI 35	29	0	0.0
ROI 8	44	17	38.6	ROI 36	20	1	5.0
ROI 9	26	7	26.9	ROI 37	16	0	0.0
ROI 10	30	6	20.0	ROI 38	30	5	16.7
ROI 11	29	8	27.6	ROI 39	28	1	3.6
ROI 12	32	10	31.3	ROI 40	16	0	0.0
ROI 13	37	6	16.2	ROI 41	17	2	11.8
ROI 14	26	6	23.1	ROI 42	16	2	12.5
ROI 15	18	1	5.6				
ROI 16	47	2	4.3				
ROI 17	40	1	2.5				
ROI 18	19	3	15.8				

ROI 19	18	2	11.1				
ROI 20	20	2	10.0				
ROI 21	22	2	9.1				
ROI 22	34	7	20.6				
ROI 23	27	3	11.1				
ROI 24	21	2	9.5				
ROI 25	9	1	11.1				
ROI 26	14	2	14.3				
ROI 27	15	2	13.3				
ROI 28	23	2	8.7				
		Average	17.8			Average	8.0

Supplementary table 2: Up and down regulated genes (excel files)